Journal of Hydrology 570 (2019) 38–50

Contents lists available at ScienceDirect

Journal of Hydrology

journal homepage: www.elsevier.com/locate/jhydrol

Research papers

Quantifying glacier mass change and its contribution to lake growths in central Kunlun during 2000–2015 from multi-source remote sensing data

Yushan Zhou[a], Jun Hu[a,*], Zhiwei Li[a], Jia Li[a], Rong Zhao[a], Xiaoli Ding[b]

[a] School of Geosciences and Info-Physics, Central South University, Changsha 410083, Hunan, China
[b] Department of Land Surveying and Geo-informatics, The Hong Kong Polytechnic University, 999077 Hong Kong, China

ARTICLE INFO

This manuscript was handled by Emmanouil Anagnostou, Editor-in-Chief, with the assistance of Eylon Shamir, Associate Editor

Keywords:
Glacier mass balance
Lake volume change
Qinghai–Tibet Plateau
SPOT-6/7 imagery
ICESat/GLA14 data

ABSTRACT

Joint monitoring of the variations of glaciers and lakes within a basin is essential for an accurate understanding of region-wide climate change and the water cycle process. The central Kunlun-KekeXili region is an ideal experimental field due to the wide distribution of glaciers and lakes. In this study, we first investigated the glacier mass balance of 2000–2015/16 for seven major glacier clusters by utilizing high-resolution SPOT-6/7 stereo imagery and the SRTM DEM. The final results revealed an overall mass balance of -0.16 ± 0.05 m w.e./a. for the study region (with a total glacier area of 967 km^2). Secondly, ICESat/GLAS altimetry data were used to quantify the water-level change of 2003–2008/09 for the two largest glacier-fed closed lakes (i.e., LexieWudan Lake and KekeXili Lake) in this region. Based on this, we applied a strategy which establishes the statistical relationship between the lake area change and the lake water-level change for 2003–2008/09 to estimate the specific water level using the corresponding lake area. We then further calculated the variation in lake water storage between 2000 and 2015. The results showed that the water storage of LexieWudan Lake and KekeXili Lake increased by 1.82 ± 0.14 km^3 and 1.90 ± 0.38 km^3, respectively. For each lake basin, meanwhile, the glaciers lost -0.18 ± 0.03 km^3 and -0.21 ± 0.04 km^3 of water, accounting for 9.9% and 11.1% of the increase in lake water storage for LexieWudan Lake and KekeXili Lake, respectively. Our results not only demonstrate that glacier meltwater has only a limited impact on the lake expansion in this region, but they also provide new evidence for the warming and wetting process of the climate in the northern part of the Qinghai–Tibet Plateau.

1. Introduction

The Qinghai–Tibet Plateau (QTP), which is also known as the "third pole" of the Earth, contains a large number of alpine glaciers and lakes, both of which are sensitive indicators of climate change. Studies have shown that glaciers across the QTP and its surroundings have experienced apparent mass loss (Yao et al., 2012; Zhou et al., 2018) since the 1970s, while most of the lakes in the interior of the QTP have been expanding (Song et al., 2013; Lei et al., 2013, 2014). After the 2000s, both the glaciers and lakes have shown an accelerated change tendency (Zhang et al., 2011; Song et al., 2013; Lei et al., 2014; Jiang et al., 2017; Kääb et al., 2015; Brun et al., 2017). Within the QTP, the variation of the glaciers and lakes not only plays an important role in regulating the regional water balance, especially for a closed lake basin, but also brings several potential risks for the ecological environment of the plateau (Tong et al., 2016). Therefore, conducting a joint investigation into the glacier mass change and lake water budget of the QTP is of great significance.

For monitoring glacier mass change, field measurement (also known as the glaciological method) is not only laborious and time-consuming, but is also a very challenging task, due to the harsh natural environment. With the rapid development of remote sensing technology, the geodetic method based on the differencing of various topography data acquired in different epochs has been widely used (Gardelle et al., 2013; Kääb et al., 2015; Brun et al., 2017, Li et al., 2017b). Compared to a considerable number of glacier investigations in the QTP's surroundings (e.g., the Himalaya/Karakoram mountains), the inner QTP glaciers have received relatively little attention, especially in the northern region. Over the whole inner QTP, geodetic-based estimates suggest that the glaciers, overall, have been in a negative state of mass budget for 2000–2016, with an apparent acceleration after 2008. For example, from a comparison of ASTER digital elevation models (DEMs), Brun et al. (2017) reported an overall mass change of -0.14 ± 0.07 m w.e./a for 2000–2016, for which the rate of mass loss increased from

* Corresponding author.
E-mail address: csuhujun@csu.edu.cn (J. Hu).

https://doi.org/10.1016/j.jhydrol.2019.01.007
Received 15 September 2018; Received in revised form 3 January 2019; Accepted 7 January 2019
Available online 10 January 2019

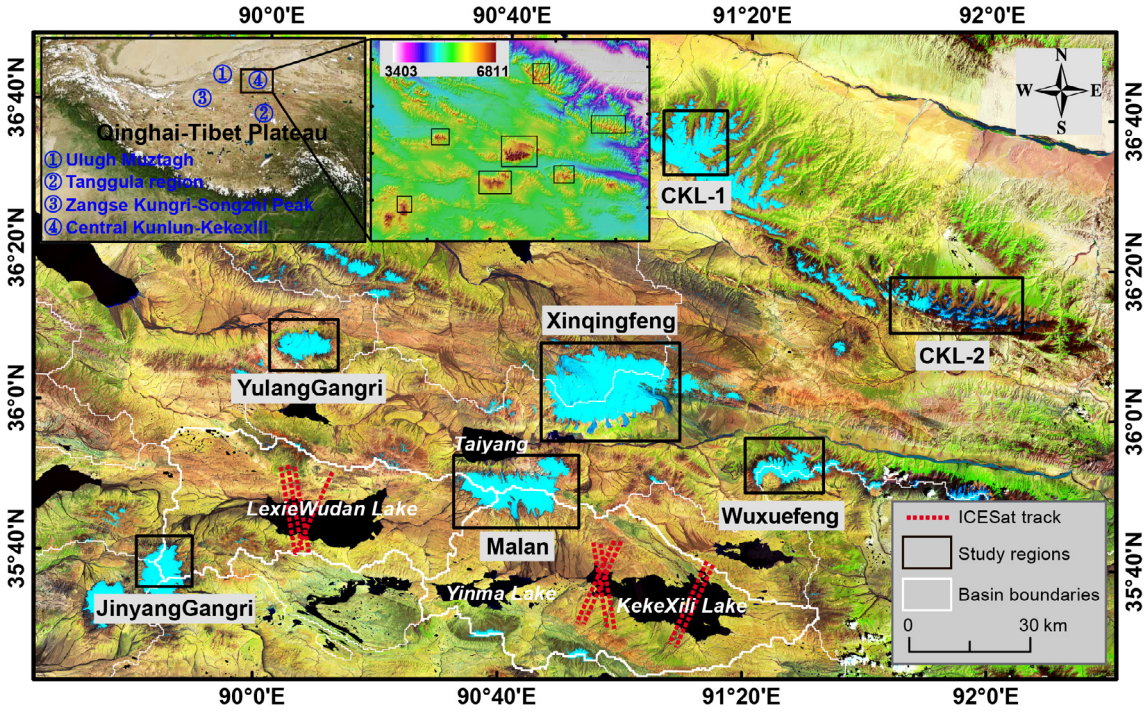

Fig. 1. Overview of the study region. The background is the Landsat 8 false-color image with a spatial resolution of 30 m. Note that CKL refers to the central Kunlun Mountain. The basin boundaries come from the HydroSHEDS (hydrological data and maps based on Shuttle Elevation Derivatives at multiple Scales) dataset (http://hydrosheds.cr.usgs.gov).

−0.01 ± 0.19 m w.e./a for 2000–2008 to −0.24 ± 0.20 m w.e./a for 2008–2016, despite a substantial overlap of error bars. Moreover, based on ICESat laser altimetry data of 2003–2008/09, Gardner et al. (2013) and Brun et al. (2017) also reported a slightly negative mass balance of −0.01 ± 0.10 m w.e./a and −0.06 ± 0.06 m w.e./a, respectively. At a sub-region spatial scale, the existing studies have revealed a strongly heterogeneous pattern of glacier mass change within the QTP. For example, the glaciers in the northwest of the QTP experienced relatively weak surface thinning (e.g., −0.07 ± 0.14 m/a over the Ulugh Muztagh region (Fig. 1) for 1975–2000) (Zhou et al., 2018) or even pronounced thickening (e.g., 0.44 ± 0.26 and 0.86 ± 0.31 m/a Zengse Kungri and Songzhi Peak for 2003–2009) (Neckel et al., 2014; Phan et al., 2017). In contrast, the central QTP (e.g., Tanggula Mountains) suffered from serious surface down-wasting, with a rate of elevation change increasing from −0.26 ± 0.14 m/a for 1976–2000 (Zhou et al., 2018) to −0.68 ± 0.29 or −0.88 ± 0.41 m/a for 2003–2009 (Neckel et al., 2014; Phan et al., 2017). In particular, in the north of the QTP (i.e., the central Kunlun-KekeXili region), the existing results of the glacier elevation change exhibited a contradictory situation, e.g., −0.90 ± 0.28 m/a in Neckel et al. (2014) versus 0.03 ± 0.47 m/a in Phan et al. (2017) for 2003–2009. However, despite being a 1° × 1° geographic grid, Brun et al.'s (2017) results implied that this region may have been in a state of mass deficit for 2000–2016. Accordingly, how the glaciers of this region respond to climate variation at a fine spatial scale is still an issue that deserves to be solved, especially considering the spatial distribution of the glaciers being relatively dispersed.

In addition, by exploying ICESat (Ice, Cloud, and land Elevation Satellite) data, previous studies have shown that the vast majority of lakes in the northern part of the QTP have experienced varying degrees of water-level rise, with the rate ranging from 0.04 m/a to 0.53 m/a for 2003–2009 (Zhang et al., 2011; Phan et al., 2012; Song et al., 2014b). Recent studies analyzing ICESat data and CryoSat-2 radar altimetry data revealed that, for the period of 2003–2014/2015, the lakes of the northern QTP, as a whole, experienced the most significant water-level rise compared to other regions within the plateau (Song et al., 2015a; 2015b; Jiang et al., 2017). For example, for KekeXili Lake and LexieWudan Lake, the two largest glacier-fed closed lakes, the rates of water-level rise increased from 0.29 m/a and 0.34 m/a for 2003–2009 (Song et al., 2014b) to 0.40 m/a and 0.45 m/a for 2010–2015 (Jiang et al., 2017), respectively. However, for the period corresponding to the glacier monitoring of this study (i.e., 2000–2015), the lake volume change, which is the most direct reflection of regional surface water storage, is still unknown, although Zhang et al. (2017) estimated the lake volume change across the whole QTP from the early 1970s to 2015. To estimate lake volume change, specific lake water levels at the beginning and end of the observation period must be known. In particular, for a study period in which lake water levels are unavailable (e.g., 2000–2015), in general, the previous studies first established a functional relationship between lake area and water level for a certain period with continuous water-level measurements (e.g., 2003–2009) by using a first-order (linear) or second-order regression model, and then calculated the unmeasured lake water levels based on the corresponding lake areas (Song et al., 2013, 2014a; Zhang et al., 2013a). Nevertheless, in this study, we directly build on the statistical relationship between lake level change and area change, to estimate the unmeasured water level and further calculate the lake volume change.

Once the lake storage change is known, we can quantitatively evaluate the contribution of glacier meltwater to lake expansion in a closed lake basin, based on an assumption that the glacier mass loss is completely transferred to the lakes (Lei et al., 2012, 2013). With regard to the causes of lake expansion, especially the contribution of glacier meltwater, Song et al. (2014b) and Zhang et al (2017), from the angle of qualitative analysis and quantitative evaluation, respectively, concluded that for the whole of the QTP glacier meltwater plays an important but not a dominant role in lake growth. In addition, for local areas, quantitative evaluations, based on either integrated physical models (e.g., hydrological models, glacier-melt models, and heat-balance equations) or an indirect estimate of glacier meltwater (based on the hypothesis mentioned above) have mainly concentrated on the central QTP, due to the abundant in-situ observation data, e.g., in Seling Co Lake (Lei et al., 2013; Tong et al., 2016) and Nam Co Lake

Table 1
Detailed information about the remote sensing data used in this study.

Satellite/sensor	Acquisition date	Path/row	B/H	Resolution	Usage
SPOT-6/7	20/09/2015 (CKL-1)		0.53	Space:	Extracting DEMs and monitoring glacier thickness change
	09/10/2015 (CKL-2)		0.55	Pan: 1.5 m; MS: 6 m	
	12/09/2015 (YulangGangri)		0.55	radiation:	
	30/11/2016 (Xinqingfeng)		0.39	12 bits	
	05/03/2016 (Malan)		0.53		
	29/02/2016 (Yuxuefeng)		0.39		
	02/11/2015 (JinyangGangri)		0.56		
Landsat 5/TM	08/05/2000	139/035		Space:	Generating lake and glacier boundaries
	19/05/2004	139/035		MS: 30 m	
	26/10/2004	139/035		radiation:	
	12/07/2006	139/035		8 bits	
	03/10/2007	139/035			
Landsat 7/ETM +	17/06/2000	139/035		Space:	
	03/10/2001*	138/035		Pan: 15 m; MS: 30 m	
	26/10/2001*	139/035		radiation:	
	16/10/2003	139/035		8 bits	
	21/10/2005	139/035			
	17/05/2006	139/035			
	02/04/2007	139/035			
	27/10/2007	139/035			
	16/12/2008	139/035			
	30/09/2009	139/035			
	02/11/2015	139/035			
Landsat-8/OLI	21/07/2015			Space:	
	09/10/2015	139/035		Pan: 15 m; MS: 30 m	
		139/035		radiation:	
				16 bits	
SRTM DEM (C-band and X-band)	02/2000			Space: 30 m	Monitoring glacier thickness change and the first-order penetration depth estimation of the C-band radar
ICESat/GLAS	2003–2009			Footprint diameter: ~70 m Sample interval: 175 m	Measuring lake water-level change

* Represents the images used as the reference for delineating glacier outlines.

(Wu et al., 2014a,b; Li et al., 2017a). However, to date, the contribution of glacier meltwater to lake water-level rise is still unclear in the north of the QTP.

In view of the above issues, the aims of this study included two main aspects. Firstly, by using SPOT-6/7 stereo imagery acquired in 2015/16 and Shuttle Radar Topography Mission (SRTM) DEMs from 2000, we generated the first high-resolution map of glacier elevation change in the central Kunlun-KekeXili region (including seven sampling regions) and obtained a region-wide glacier mass change figure based on the geodetic method. Secondly, we estimated the water storage change of two typical glacier-fed closed lakes (i.e., LexieWudan Lake and KekeXili Lake) between 2000 and 2015 using the strategy mentioned above. We then roughly quantified the contribution of glacier meltwater to the lake expansion based on the assumption mentioned above. The results of this work will help to improve the understanding of the responses of glaciers and lakes to climate change and the relationship between them in the northern part of the QTP.

2. Study region

The central Kunlun-KekeXili region is located in the north of the QTP, with an average altitude of above 5000 m. Owing to the harsh natural environment characterized by a cold and dry climate, this area is sometimes referred to as “no man’s land”. On this plateau, the mean annual air temperature is, on average, about −10 °C, and the annual precipitation is 173–494 mm (Li et al., 1996). More than 90% of the precipitation occurs from May to September, implying that the glaciers in this region belong to the summer-accumulation type. In addition, affected by the intense westerly winds, this area is one of the regions with the highest wind speed in the entire QTP (Li et al., 1996). Furthermore, throughout the whole region, the terrain is relatively flat and there are some scattered mountains, among which the highest peak is Xinqingfeng Mountain with an altitude of about 6800 m (Fig. 1). In these high altitudes, the glaciers and ice caps are fully developed and together cover a total area of 1810 km^2 in the northern part of the QTP. From optical images, it appears that the glacier surface are relatively clean and that debris is almost non-existent. In addition, there are a large number of alpine lakes of all shapes and sizes in this region. Of these lakes, KekeXili Lake and LexieWudan Lake, which both cover an area of more than 200 km^2, are the largest glacier-fed endorheic lakes. In particular, over the LexieWudan basin, the minimum distance from glacier front to lake inlet is only about 20 km. This is thus an ideal experimental region for evaluating the response of lakes to glacier changes. In the KekeXili basin, the water from Yinma Lake seasonally overflows into KekeXili Lake. In addition, these three lakes, despite being located in adjacent areas, have different phenological features, possibly due to the differences in hydrochemical characteristics, bathymetry, and lake shape (Yao et al., 2013).

3. Dataset

3.1. SPOT-6/7 imagery

As an extension of the SPOT mission, two advanced satellites—SPOT-6 and SPOT-7 (pushbroom imaging systems) were successfully launched on September 9, 2012, and June 7, 2014. Both satellites were designed with the same orbit setting (sun-synchronous orbit with a 98.2° inclination at an altitude of 694 km) and phased 180° from each other, allowing the satellites to revisit anywhere with a minimum period of one day. The panchromatic and multispectral images are acquired simultaneously with a ground sample distance (GSD) of about 2.1 m and 8.4 m (nadir condition), corresponding to a nominal resolution of 1.5 m and 6 m by oversampling processing in the ground segment (SPOT-6/7 User Guide). The radiometric coding of the images is 12 bits, which is higher than that in the previous SPOT series satellites. Benefiting from the exceptional agility of the telescope

instrument, the two satellites can offer a flexible base-to-height (B/H) ratio to generate stereo or tri-stereo data. Over the QTP, they have been successfully used to estimate glacier elevation changes (Ragettli et al., 2016; Kääb et al., 2018). In this study, we selected the classic stereo mode (forward and backward viewing geometry) with a B/H ratio between 0.39 and 0.56 (Table 1). All of these images have had radiometric and sensor distortion corrections performed.

3.2. Landsat 5/7/8 imagery

We collected a total of 18 Landsat images (five scenes for Landsat 5, 11 scenes for Landsat 7, and two scenes for Landsat 8) to retrieve the time-series lake boundaries and to provide a reference for the glacier outlines in 2000. Because of the Scan Line Corrector (SLC) failure of the Landsat 7 satellite on May 30, 2003, the Landsat 7 images have contained wedge-shaped data gaps since that date, causing approximately 22% data loss for each scene. All of the images we used belonged to the highest-quality Level 1 Precision Terrain (L1TP) data. Due to that the geo-registration accuracy of the data is better than 12 m, they can be directly used to perform a pixel-level time-series analysis (https://landsat.usgs.gov/landsat-collections). Moreover, regarding the issue of data selection, a vital and universal criterion is that the fraction of cloud coverage in the optical images should be as small as possible, especially over the glaciers and lakes, as well as their nearby zones. More concretely, for glacier areas, we should avoid utilizing images affected by heavy seasonal snowfall, which can make it difficult to distinguish exact glacier outlines. For lake areas, in order to obtain more accurate boundaries, we chose images acquired in the non-freezing period. With regard to the few images inevitably contaminated by cloud, we employed the images close to their acquisition dates to assist with the complete delineation of lake/glacier boundaries. Details are given in Table 1.

3.3. SRTM DEM

In this study, we used the SRTM 1 arc-second (~30 m) global elevation data (SRTM-GL1) from the U.S. Geological Survey to investigate the glacier elevation change. Compared to the raw data products, the voids of this dataset have been filled (but may still exist in some areas). By checking the SRTM non-void-filled elevation data, we found that this study region is not affected by data gaps. Moreover, the SRTM X-band DEMs released by the DLR with a spatial resolution of ~25 m (Ludwig and Schneider, 2006) were used to estimate the first-order approximation of the penetration depth of the C-band radar. For technical reasons, the swath width of the SRTM X-band DEM is limited to 50 km, resulting in incomplete data coverage for the land surface (Roth et al., 2001). For example, in the YulangGangri Ice Cap and the Xinqingfeng and Malan mountains, the X-band DEM data are unavailable. It should be noted that the SRTM C-band DEM provides the orthometric height with the EGM96 geoid as the vertical datum, while the X-band data represent the ellipsoid height with respect to WGS84. For the horizontal datum, they are both referenced to the WGS84 ellipsoid (Farr et al., 2007).

3.4. ICESat/GLAS elevation data

The ICESat satellite launched in January 2003 is the first spaceborne laser altimeter mission and its main payload is the Geoscience Laser Altimeter System (GLAS) instrument (with a pulse wavelength of 1064 nm) (Zwally et al., 2002; Zhang et al., 2011). ICESat data are acquired in the form of a footprint (or facula) with a nominal diameter of ~70 m (in practice with a size of 50–105 m) sampled at a spacing of about 172 m along the track (Zwally et al., 2002; Duan and Bastiaanssen, 2013). Due to the design of the polar orbit, the ICESat sample track is relatively sparse at low and middle latitudes (e.g., the QTP), with a cross-track distance ranging from hundreds of meters to dozens of kilometers. In addition, studies have proven that ICESat/GLAS elevation data have an excellent altimetry and geolocation accuracy, corresponding to decimeter and meter levels, respectively (Zwally et al., 2002, 2008; Phan et al, 2012; Zhang et al., 2013b). Hence, ICESat/GLAS elevation data have been widely used for monitoring the fluctuation of inland lake water levels (Zhang et al., 2011, 2013b; Phan et al., 2012; Song et al., 2013). In the present study, we exploited the latest version L2-level altimeter product (GLA14; Release 34), which can be freely downloaded from the National Ice and Snow Data Center (NISDC). The data are referenced to the TOPEX/Poseidion ellipsoid and EGM 2008 geoid.

4. Data processing

4.1. Glacier change estimation

4.1.1. Glacier boundaries

In this study, we did not generate our own glacier outlines, but directly used the Second Chinese Glacier Inventory (CGI-2, version 1.0) (Liu et al., 2014), which was produced based on Landsat TM/ETM+ images taken mainly during 2006–2010 (Guo et al., 2015). The position accuracy of the CGI-2 boundaries is about ± 10 m for manually revised clean-ice outlines (Guo et al., 2015). Over this study area, the CGI-2 outlines represent the glacier extent in 2005. In consideration of possible glacier advance and retreat within our study period, we manually edited the CGI-2 boundaries to obtain the most extensive glacier extent by reference to the Landsat 5 TM images from 2000 and the orthorectified SPOT-6/7 images from 2015/16. Furthermore, based on the final glacier elevation change map, we made a slight adjustment for the boundaries in the accumulation zones (only for Xinqingfeng and Malan mountains).

4.1.2. SPOT-6/7 DEM generation

We processed all of the SPOT-6/7 stereo images via the OrthoEngine module of PCI Geomatica 2014. Due to that there are no in-situ ground control points (GCPs) in this study region, we chose to automatically collect the GCPs from the SRTM C-band DEM. To be specific, the first step was to orthorectify the SPOT-6/7 panchromatic images (with a resolution of 1.5 m) by utilizing the SRTM data. The second step was to implement an automatic GCP collection program in the PCI Geomatica software, with the orthorectified image and the SRTM DEM as the horizontal and vertical references, respectively. Meanwhile, in order to improve the accuracy of the stereo model, between 30 and 48 tie points (TPs) used for assisting the orientation were automatically identified based on the correlation matching technique (Table 2). We found that it was very necessary to visually check every GCP and TP. We first removed some GCPs measured in glacier areas and mountain ridges/valleys with possibly inaccurate elevation information. Similarly, some TPs located in the vicinity of cloud and shadow were also discarded (only for the EKL-1 and EKL-2 regions). The final model residuals in the image space were below 0.52 pixels (Table 2). Finally, the extracted DEMs were resampled to the 30-m resolution in UTM projection and a median filter was carried out with a sample window of 3 × 3.

4.1.3. DEM differencing

With regard to the differencing process for the DEMs, we mainly followed the strategy of Zhou et al. (2017, 2018). Specifically, we first employed the classic three-dimensional registration method proposed by Nuth and Kääb (2011) to make the SRTM DEMs match the SPOT-6/7 DEMs. Subsequently, we checked and corrected the maximum curvature-, elevation-, slope-, and aspect- dependent biases by applying the fitted polynomial based on the statistics over ice-free regions to the glacier areas. In addition, given the fact that for this pushbroom-type sensor, weak variations of the satellite attitude (caused by slight jitter) can induce bias along the direction of the flight and/or cross-track in the resulting DEM products (Berthier et al., 2007; Leprince et al., 2007;

Table 2
The aerial triangulation information and the statistics of elevation differences over the ice-free areas. Note that STD denotes the standard deviation. NMAD is the abbreviation for normalized median absolute deviation (Höhle and Höhle, 2009).

Region	No. GCPs	No. TPs	Residual(pixel)	Statistics of elevation differences over ice-free areas (after correction) (m)				
				Mean	Median	STD	NMAD	No. Samples
CKL-1	5	39	0.38	0.11	−0.04	11.05	5.73	96,688
CKL-2	14	30	0.52	0.24	0.36	7.46	3.36	204,712
YulangGangri	32	47	0.22	−0.10	−0.12	3.89	2.19	185,664
Xinqingfeng	26	48	0.48	0.08	0.10	3.29	2.39	549,226
Malan	28	45	0.29	−0.01	0.01	3.90	2.30	503,286
Yuxuefeng	25	44	0.24	−0.03	−0.06	4.05	2.39	201,514
JinyangGangri	28	48	0.37	0.00	−0.11	3.89	2.95	137,335

Nuth and Kääb, 2011), by visually checking the final elevation difference maps, we did not find along- or cross-track bias. Finally, for pixels whose values are larger than the three-fold standard deviation of glacier elevation change of the altitude band they belong to, we removed them as outliers. As for the ice-free areas, the detailed statistics are given in Table 2.

4.1.4. Estimation of the penetration depth difference between the SRTM C-band and X-band DEMs

In general, since C-band radar can penetrate into glacier ice by up to 1–2 m and into dry snow by up to 10 m (Rignot et al., 2001), in order to more accurately quantify the glacier thickness changes, the impact of the penetration depth needs to be eliminated as much as possible, especially for snow-covered areas. In this study, following the method of Gardelle et al. (2013), we provided the first-order approximate estimate of the C-band penetration depth by subtracting the SRTM C-band DEM from the X-band DEM. Details of the data processing can be found in Zhou et al. (2018). It should be emphasized that the penetration depth we obtained actually represents the penetration depth difference between C-band and X-band radar, as the X-band radar can also penetrate into dry snow by up to 2–6 m (Dehecq et al., 2016; Round et al., 2017; Lambrecht et al., 2018; Kääb et al., 2018). Based on the elevation difference map, a penetration depth difference curve as a function of altitude was obtained, and was then used to perform the correction for each pixel in the glacier areas. For the JinyangGangri Ice Cap, the SRTM X-band DEM does not cover the whole study region, resulting in no penetration depth corrections at high altitudes (above 5700 m). Given that the obtained penetration depth difference basically showed a linear trend (Fig. 2), we linearly extrapolated the curve to the unmeasured zones and obtained a region-wide average penetration difference of 3.14 m, which is slightly higher than the original result of 2.26 m. In addition, for regions where the SRTM X-band DEMs are unavailable (such as the Xinqingfeng, Malan, and YulangGangri regions), we did not follow the frequently used strategy of employing the average penetration corrections in the nearby regions (Gardelle et al., 2013), but instead adopted the penetration trend of the adjacent areas and further made a reasonable adjustment (referring to linear extrapolation in accordance to the corresponding glacier hypsometry). Our strategy should be more reasonable, as it takes into account the difference in glacier hypsometry for different regions. To be specific, the penetration trend in Wuxuefeng Mountain was used to estimate the corrections for Xinqingfeng and Malan mountains. For the YulangGangri Ice Cap, the result for the JingyangGangri Ice Cap was employed. The final average penetration depth differences were 3.43 m for Qinqingfeng Mountain, 3.26 m for Malan Mountain, and 2.55 m for the YulangGangri Ice Cap (Table 3).

4.1.5. Calculation of geodetic mass balance and uncertainty assessment

To calculate the mass balance, the first step was to obtain the glacier hypsometry and to generate a glacier thickness change curve as a function of altitude for each sub-region. For the data gaps in the elevation difference map, they were filled by the average elevation change calculated by valid pixels in the same altitude band. The region-wide volume change could then be obtained by an integral operation of the thickness change and the area for each altitude interval. Ultimately, a conversion factor of 850 ± 60 kg/m^3 was used to translate the volume change into mass change (Gardelle et al., 2013; Huss, 2013). In particular, given that the pattern and magnitude of elevation change of the surge-type glaciers were totally different from those of the non-surge-type glaciers, their mass balances (b) were separately calculated using Eq. (1) and added to the final region-wide results based on an area-weighting strategy.

$$b = \frac{f_c(\sum r^2 \Delta h)}{s} \tag{1}$$

where r is the spatial resolution of the elevation difference map (30 m), and $\Delta h$and s respectively represent the thickness change of each pixel and the glacier area for a given glacier.f_c denotes the conversion coefficient (0.85 ± 0.06).

To evaluate the total uncertainty of the mass balance, the random error and systematic error need to be considered comprehensively. For the random error, we first took into account the uncertainty of the glacier thickness change, which mainly depended on the errors of the DEMs and the penetration depth difference estimation. In fact, the latter also depends on the DEM error, as it was determined by the differencing of the DEMs. Given the fact that high altitudes in this study area are almost completely covered by ice and snow, we used the standard deviation of the elevation difference of the entire ice-free area to represent the uncertainties of the glacier elevation change and penetration difference estimation for each altitude band. Furthermore, in order to consider the influence of spatial autocorrelation between DEMs, we fitted an experimental semivariogram using a spherical model in ice-free regions. The obtained autocorrelation distance ranges from 80 m to 240 m for the penetration depth difference maps, and from 150 m and 330 m for the glacier elevation difference maps. Considering that glacier areas generally have a higher autocorrelation than stable regions (Rolstad et al., 2009), we conservatively assumed that the autocorrelation distance in glacier areas was four times that in ice-free regions. The uncertainty of the glacier thickness change ($\sigma_{\Delta h}$) for each altitude band (i) was then calculated by Eqs. (2)–(4):

$$\sigma_{\Delta h,i} = \sqrt{\left(\frac{\sigma_g}{\sqrt{N_{effg,i}}}\right)^2 + \left(\frac{\sigma_p}{\sqrt{N_{effp,i}}}\right)^2} \tag{2}$$

$$N_{effg,i} = \begin{cases} 1, N_{effg,i} \le 1 \\ \frac{N_t \times r^2}{\pi \times (4d_g)^2}, N_{effg,i} > 1 \end{cases} \tag{3}$$

$$N_{effp,i} = \begin{cases} 1, N_{effp,i} \le 1 \\ \frac{N_t \times r^2}{\pi \times (4d_p)^2}, N_{effp,i} > 1 \end{cases} \tag{4}$$

where σ denotes the standard deviation of the elevation difference in

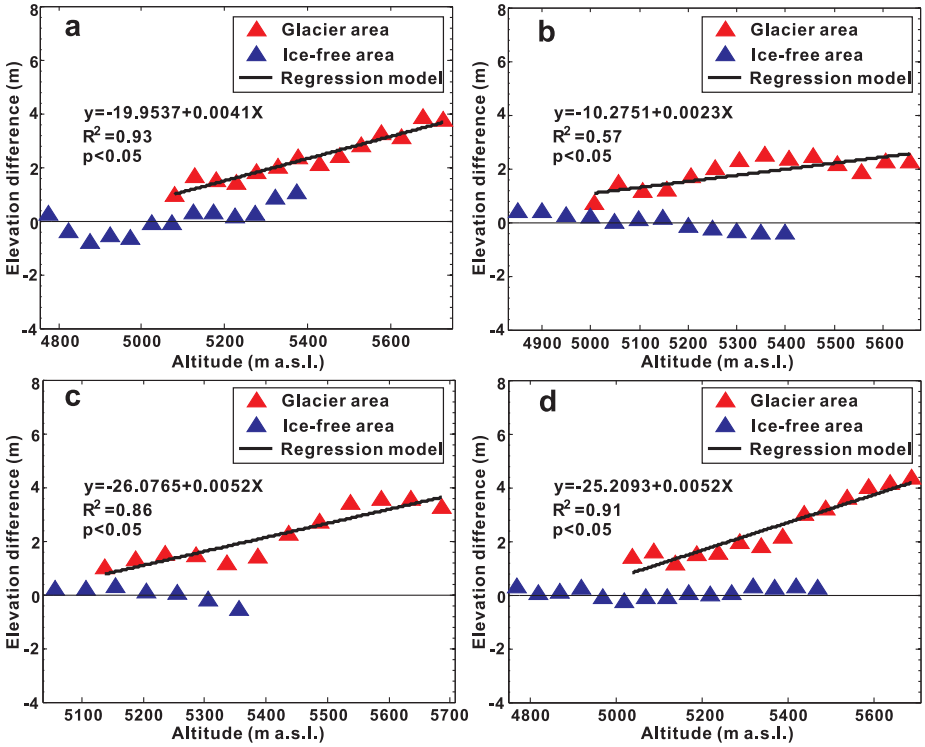

Fig. 2. The elevation change between the SRTM C-band and X-band DEM for each 50-m altitude band. (a) CKL-1. (b) CKL-2. (c) JinyangGangri Ice Cap. (d) Wuxuefeng Mountain.

the ice-free regions, and the subscripts "p" and "g" represent the glacier elevation difference map and the penetration depth difference map, respectively. $N_{eff\,g,i}$ and $N_{eff\,p,i}$ denote the number of independent observations for each elevation band. N_t is the total number of observations for a given altitude interval. d_g and d_p denote the autocorrelation distance for non-glacier areas. The uncertainties of the volume change ($\sigma_{\Delta V}$) and the mass balance ($\sigma_{\Delta m,rdn}$) were then respectively calculated by Eqs. (5)–(7), based on the strategy of Zhou et al. (2018):

$$\sigma_{\Delta V} = \sqrt{\sum_{i=1}^{n} (\sigma_{\Delta h,i} \times S_i)^2} \tag{5}$$

where S_i is the glacier area for each altitude band.

$$\sigma_{\Delta m0} = \sqrt{\left(\frac{\Delta V \times \sigma_{\Delta f}}{S_t}\right)^2 + \left(\frac{\sigma_{\Delta V} \times \Delta f}{S_t}\right)^2 + \left(\frac{\Delta V \times \Delta f \times \Delta S}{S_t{}^2}\right)^2} \tag{6}$$

where $\sigma_{\Delta f}$ is the uncertainty of the conversion factor (60 kg/m^3). ΔS is the uncertainty of the glacier boundaries, which was assumed to be an error of 10% in this study (Maurer et al., 2016). S_t is the total glacier area for each investigated region. $\sigma_{\Delta m0}$ refers to the initial mass balance uncertainty.

$$\sigma_{\Delta m,rdn} = \sqrt{\sigma_{\Delta m0}{}^2 + \sigma_{abs\_p}{}^2} \times \frac{1}{1 - P_{void}} \tag{7}$$

where σ_{abs_p} represents the uncertainty caused by the absolute penetration depth of the C-band radar (i.e., considering the uncertainty induced by the penetration depth of the X-band radar). In this study, we conservatively assumed that this was in the order of 1.5 m, corresponding to a mass change of 1.28 m w.e. (Gardelle et al., 2013). P_{void} denotes the proportion of data voids for each region (Fig. 4). The aim of introducing this term was to consider the uncertainty caused by the data gaps. More details concerning the accuracy evaluation can be found in Zhou et al. (2018). In addition, it should be highlighted that we did not take the influence of seasonal snowfall into account this study, as the images we used were acquired mainly from September to March, where the precipitation can be considered negligible. Furthermore, for the systematic error, we used the absolute mean of the elevation differences in ice-free area to approximately represent it. The corresponding mass balance uncertainties ($\sigma_{\Delta m,sys}$) are between 0.00 and 0.20 m w.e. (Table 2). Finally, the total uncertainty of the mass balance ($\sigma_{\Delta m}$) can be obtained by Eq. (8).

$$\sigma_{\Delta m} = \sqrt{\sigma_{\Delta m,rdn}{}^2 + \sigma_{\Delta m,sys}{}^2} \tag{8}$$

4.2. Lake change estimation

4.2.1. Lake boundary extraction

We first filled the data gaps in the Landsat 7/ETM + images using a simple toolbox (Landsat Gapfill) in ENVI software. A band ratio method (band 4/band 5 for Landsat 5/7 TM/ETM + images, band 5/band 6 for Landsat 8 OLI images) with an empirical threshold of 2.0 was then applied to automatically identify the lake outlines (Li et al., 2017a). The initial lake boundaries were then refined by visually comparing the Landsat false-color images (RGB: bands 5/4/3). For some images more or less contaminated by cloud, we made a further revision in local zones of the lake boundaries by reference to the multi-temporal Landsat images. Moreover, since LexieWudan Lake merges with several nearby

Table 3
The first-order approximation of the penetration depth of C-band radar in the central Kunlun-KekeXili region (unit: meter).

Region	CKL-1	CKL-2	Wuxuefeng	Xinqingfeng	Malan	YulangGangri	JinyangGangri
Average penetration depth difference (m)	2.12	1.82	2.76	3.43	3.26	2.55	3.14

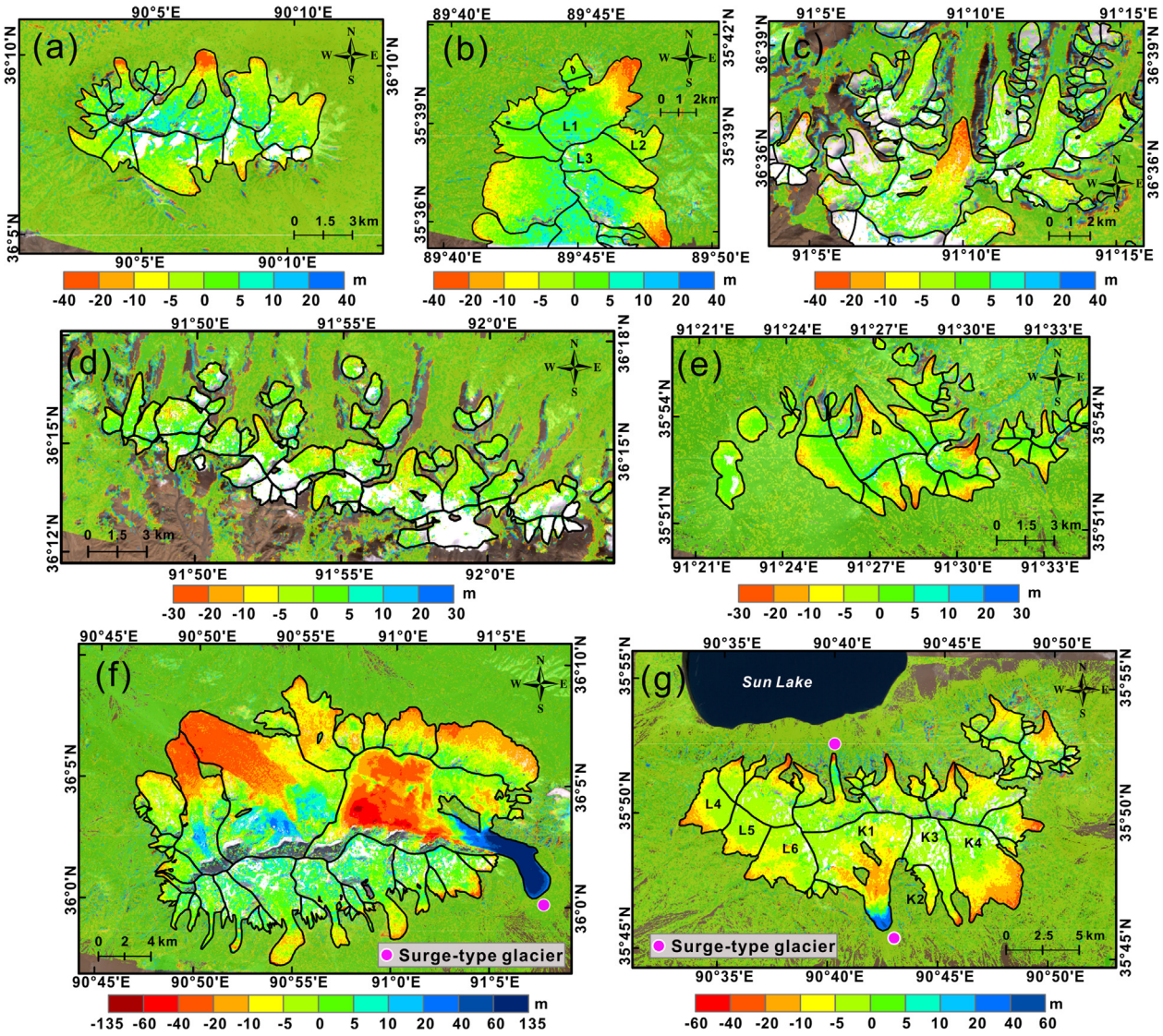

Fig. 3. Glacier thickness changes for 2000–2015/16 in the central Kunlun-KekeXili region. Note that the red circles denote the glaciers in the surge phase during our study period. (a) YulangGangri Ice Cap. (b) JinyangGangri Ice Cap. (c) CKL-1. (d) CKL-2. (e) Wuxuefeng Mountain. (f) Xinqingfeng Mountain. (d) Malan Mountain. (For interpretation of the references to color in this figure legend, the reader is referred to the web version of this article.)

small lakes during its expansion, in the course of editing the lake boundaries, we excluded these lakes when they were completely separated, but included them when they merged into one lake (Fig. S1).

4.2.2. ICESat/GLAS data processing, lake water volume change estimation, and uncertainty assessment

In order to ensure the consistency of the reference datum, we first transformed the TOPEX/Poseidon ellipsoid and EGM2008 geoid into the WGS84 ellipsoid and EGM96 geoid, respectively. We then took the saturation correction of the GLAS detector into consideration, as specular reflection occurring on a flat lake surface easily induces distortion of the altimetry echo pulses. In this study, the average saturation correction was about 0.40 m, with a maximum of 1.38 m. For some footprints whose saturation correction values were characterized by "−999" (suggesting that these points need to be corrected but do not have valid correction values), they were excluded to avoid introducing potential bias (Abdallah et al., 2011). The performance of the saturation correction is shown in Fig S2. Subsequently, we employed a two-step procedure to check and remove outliers (Zhang et al., 2011). The first step was to remove the gross error possibly induced by the cloud coverage, based on a visual inspection. However, in this study, we did not find this type of error. Next, in consideration of the vertical accuracy of the ICESat/GLAS altimetry data, we set a threshold of standard deviation of 15 cm to remove some footprints causing a large deviation (Fig. S2).

After performing the above corrections, the ICESat footprints were used to analyze the lake water-level change for 2003–2008/09. To obtain the lake volume change within the study period, the lake water levels for 2000 and 2015 were needed. Given that a rise of lake water level is generally expressed by the expansion of the lake area, there may be a certain relationship between the lake water-level change and the lake area change. Let us imagine that a lake can be approximately represented by a bowl. When the water level rises by Δh, from a vertical section, a functional relationship $\Delta h = \Delta x \cdot \tan(\theta)$ can be easily established, where θ denotes the slope and Δx represents the horizontal displacement of the boundary caused by the surface expansion. However, in practice, since the lake shape and the horizontal displacement of the boundary are not regular and highly variable (Fig. S1), the lake area change can be expressed by a generalized function: $\Delta S = F(\Delta x)$. Based on this, the relationship between the lake water-level change and the area change can be established by $\Delta h = F^{-1}(\Delta S) \cdot \tan(\theta)$. In addition, as the change could be positive (increase) or negative (decrease), the

functional model can be further extended as $|\Delta h| = F^{-1}(|\Delta S|)\bullet\tan(\theta)$. Thus, we can use regression analysis to establish the relationship between the area change and the water-level change (in an absolute sense), assuming that the mean slope of the terrain around the lakes is a constant varying with the lakes. It should be noted that, in this study, we only retrieved the lake boundaries for the times with significant water-level fluctuations (i.e., in late spring/early summer and autumn) and performed the differencing operation in pairs of two arbitrary measurements to build the statistical relationship between the lake level change ($|\Delta H|$) and area change ($|\Delta S|$). According to the established statistical model, we could extrapolate the lake water level using the lake areas for 2000 and 2015, and further estimate the lake water volume change (ΔV_{Lake}) using Eq. (9) (Lei et al., 2013; Tong et al., 2016).

$$\Delta V_{Lake} = \frac{1}{3}(H_2 - H_1) \times (\sqrt{A_1 \times A_2} + A_1 + A_2) \tag{9}$$

where H and A denote the lake water level and lake area, respectively. The subscripts "1″ and "2" represent the beginning and the end observation times.

To evaluate the accuracy of the lake volume change, we used the prediction interval of the regression model to approximately represent the uncertainty of the extrapolated water level (σ_H). With regard to the uncertainty of the lake area (σ_S), it was calculated by the product of the lake perimeter and the image resolution (15 m), based on an assumption of one pixel error for the lake boundary. Finally, according to error propagation law, the uncertainty of the lake volume change ($\sigma_{\Delta V_{lake}}$) was obtained by Eq. (10), supposing that the error of each term in Eq. (9) follows a Gaussian distribution.

$$\sigma_{\Delta V_{Lake}} = \sqrt{\frac{1}{9}(\sqrt{A_1 A_2} + A_1 + A_2)^2(\sigma_{H_2}{}^2 + \sigma_{H_1}{}^2) + \frac{1}{36}(H_2 - H_1)^2\left[\left(\sqrt{\frac{A_2}{A_1} + 1}\right)^2 \sigma_{S_1}{}^2 + \left(\sqrt{\frac{A_1}{A_2} + 1}\right)^2 \sigma_{S_2}{}^2\right]} \tag{10}$$

5. Results

5.1. Glacier thickness change and mass balance

From Fig. 3, it can be seen that almost all of the glaciers among the investigated areas experienced different degrees of surface thinning near their toes, except for the surging glaciers. Based on the median elevation of each glacier from the Randolph Glacier Inventory (RGI) Version 6.0 (RGI Consortium, 2017), we approximately estimated the position of the region-wide glacier equilibrium line by using the mean of them and further divided glaciers areas into two parts—the ablation zones and the accumulation zones (Fig. 4). To be specific, for the ablation zones, the highest rate of surface down-wasting of -0.51 ± 0.05 m/a appeared in the Xinqinfeng region, followed by the Malan and Wuxuefeng regions with a value of -0.47 ± 0.06 m/a and -0.43 ± 0.10 m/a, respectively. The other regions also exhibited pronounced surface lowering, ranging from -0.26 ± 0.06 m/a to -0.18 ± 0.06 m/a. For the accumulation zones, the Malan and Wuxuefeng regions showed slight thinning at a rate of -0.05 ± 0.08 m/a and -0.06 ± 0.06 m/a, respectively, while the CKL-2 exhibited a nearly stable condition (0.00 ± 0.20 m/a). The rest of areas showed different degrees of thickening, ranging from 0.06 ± 0.28 m/a to 0.24 ± 0.07 m/a.

Synthesizing all the glacier changes over all the sample sites (with a total glacier area of 966.7 km^2) shows an area-weighted mass balance of -0.16 ± 0.05 m w.e./a for 2000–2015, which is equivalent to a mass loss of -0.16 ± 0.05 Gt/a. Across the entire region, the pattern of glacier mass change is heterogeneous. The highest rate of mass loss occurred in the Malan and Xinqinfeng mountains, with mass budgets of -0.22 ± 0.10 and -0.21 ± 0.10 m w.e./a, followed by the Wuxuefeng region, with -0.16 ± 0.10 m w.e./a. The JinyangGangri, CKL-1, and CKL-2 regions have been in a state of slightly negative budget, corresponding to mass changes of -0.04 ± 0.09, -0.08 ± 0.21, and -0.09 ± 0.16 m w.e./a, respectively. In particular, an approximately balanced condition (0.01 ± 0.11 m w.e./a) can be found in the YulangGangri Ice Cap.

5.2. Lake water-level changes (2003–2008/09 and 2000–2015)

From Fig. 5 (the left pictures), the rates of lake water-level rise for 2003–2008/09 are 0.36 m/a and 0.31 m/a for LexieWudan Lake and KekeXili Lake, respectively. This is in agreement with previous results for the same period (about 0.34 m/a and 0.29 m/a) (Phan et al., 2012; Wang et al., 2013; Song et al., 2014b). Interestingly, the water level exhibited a stable and continuous increase each year in LexieWudan Lake, but showed a significant increase every two years in KekeXili Lake. Moreover, in accordance with the selected ICESat data and the corresponding lake areas (Table S1), the statistical model and lake water-level changes for 2000–2015 are shown in Fig. 5 (the middle and right pictures). In the whole study period, the water level of LexieWudan Lake basically exhibited a monotonous increase, with a mean increase rate of 0.49 m/a (corresponding to an overall rise of 7.40 m), for which the rates of the two sub-periods (2000–2007 and 2007–2015) were 0.50 m/a (3.52 m) and 0.49 m/a (3.88 m), respectively. In contrast, KekeXili Lake reflected a mean rate of water-level rise of 0.38 m/a (5.76 m) for 2000–2015. Comparing the results of the two sub-periods indicates that the rate of water-level rise increased by 100% from 0.26 m/a (1.8 m) for 2000–2007 to 0.50 m/a (3.96 m) for 2007–2015. Furthermore, in order to better validate the performance of our model, we compare our results with those obtained by Jiang et al. (2017) using CryoSat-2 data. It is evident that the CryoSat-2 results are consistent with our estimated trend in KekeXili Lake, but are slightly higher than that in LexieWudan Lake (Fig. 5). This may be caused by the systematic bias between the two datasets (Song et al., 2015b; Crétaux et al., 2016).

5.3. Lake volume change and the contribution of glacier meltwater to lake expansion

For 2000–2015, the estimated lake water volume changes are 1.82 ± 0.14 km^3 and 1.90 ± 0.38 km^3 in LexieWudan Lake and KekeXili Lake, respectively. Summing up the volume changes of each individual glacier within the respective lake basins gives a volume change of -0.18 ± 0.03 km^3 and -0.21 ± 0.04 km^3 (Figs. S3 and S4). Under the simple hypothesis that all of the lost water in the glacier systems flows into the lakes (without consideration of evaporation/sublimation or the wastage in the course of transport), the glacier mass loss respectively accounts for 9.9% and 11.1% of the lake growth in LexieWudan Lake and KekeXili Lake. In particular, an additional assumption that Yinma Lake has been in balance during 2000–2015 is needed for the KekeXili basin, given the fact that the lake extent is unchanged.

6. Discussion

6.1. The impact of penetration depth on glacier mass change

Since the penetration depth of the X-band radar was not considered, the penetration depth of the C-band radar we obtained is likely underestimated. Prior studies have shown that, for dry snow, the penetration depth of X-band radar can reach 2–6 m in Antarctica (Groh et al., 2014; Seehaus et al., 2015; Zhao and Floricioiu, 2017) and 4–6 m in the Alps (Berthier et al., 2016; Dehecq et al., 2016). Especially in the QTP and its surroundings, the X-band average penetration depth in the accumulation zone is about 2 m or less in the Karakoram mountain (Round et al., 2017), 3 m in the western Tibet (Kääb et al., 2018) and 3–4 m in the central Pamir (Lambrecht et al., 2018). These imply that

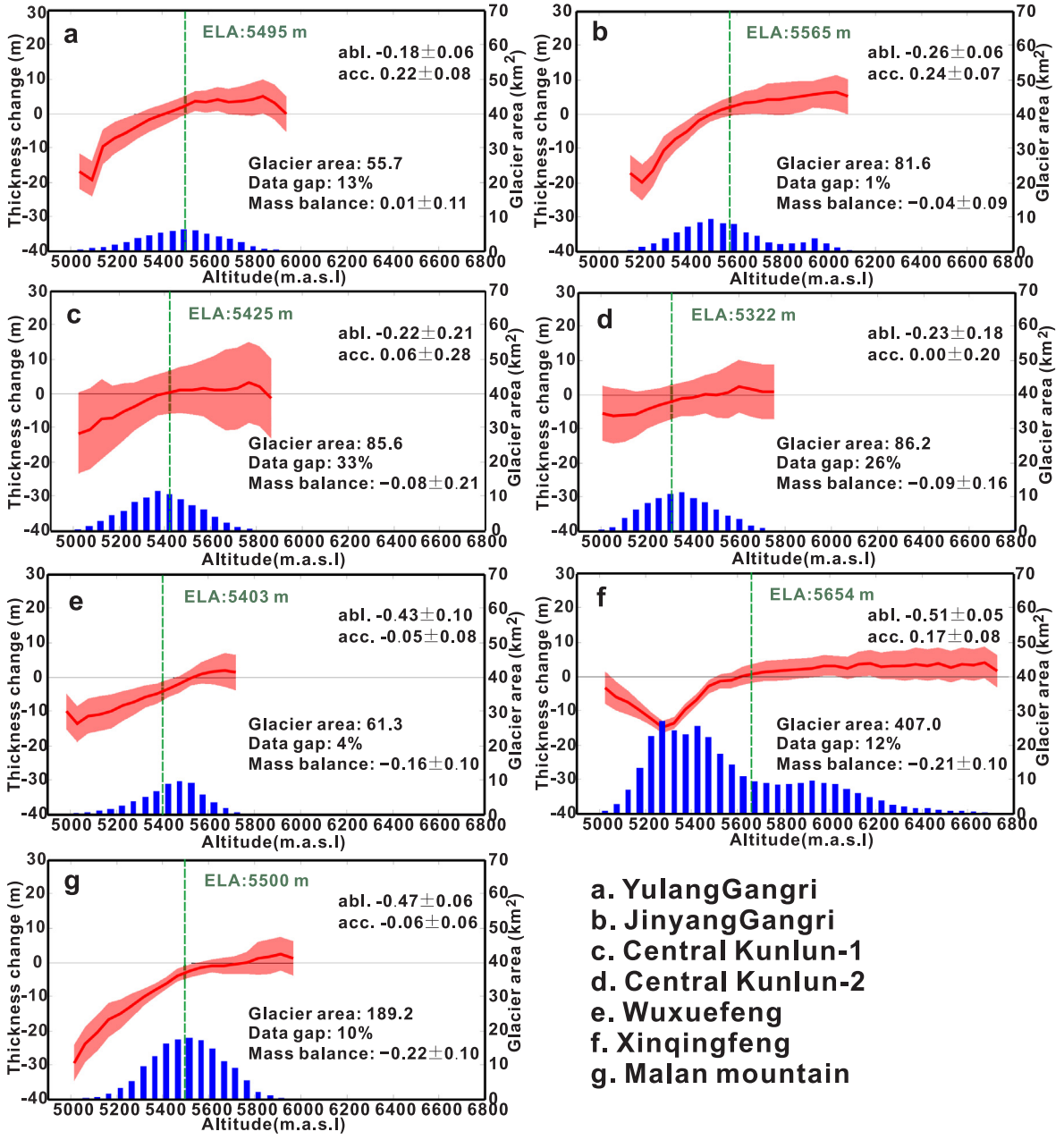

Fig. 4. Region-wide glacier hypsometry and thickness change curve with an altitude bin of 50 m. The area shaded in red indicates one standard deviation of the glacier elevation change within a given altitude band. The terms "abl." and "acc." refer to the ablation and accumulation zones, and the values next to them represent the glacier thickness change (unit: m/a). In addition, the units of glacier area and mass balance are km^2 and m w.e./a, respectively. (For interpretation of the references to color in this figure legend, the reader is referred to the web version of this article.)

the uncorrected X-band penetration depth may introduce significant bias into the final mass balance estimation, if there is a large amount of dry snow. However, the precipitation in this region is sparse, especially in winter (the season of SRTM acquisition). Xie et al. (2000) reported that the amount of annual precipitation (in the form of snowfall) is only about 400–500 mm in the altitude of the glacier equilibrium line in the Malan region. We can thus intuitively speculate that the thickness and extent of the dry snow may be limited in this area. In addition, in order to better elaborate this issue, we generated a complimentary result by considering the penetration depth of the X-band radar (assuming an average of 1.5 m for the entire glacier area (Gardelle et al., 2013)). The updated results are more negative by 0.08 m w.e./a than our results, but the two results agree within the error bounds (Fig. 6). Furthermore, under the hypothesis of the average penetration depth of X-band radar being 4 m, the setting of this study (1.5 m) actually means that the coverage ratio of dry snow reaches about 40% in this region. Intuitively, this ratio may be rational or even overestimated. This is because, with the increase of altitude, the accumulation zones consist of superimposed ice zones, wet-snow zones, percolation zones, and dry snow zones, in sequence (Xie and Liu, 2010). A 40% ratio of dry snow (with an average thickness of 4 m) seems to be high, given the currently known climate conditions. From another point of view, the maximum penetration depth obtained by the extrapolation in this study is about 9 m in the Xinqingfeng region, which is very close to the 10 m maximum penetration of C-band radar for dry snow (Rignot et al., 2001). This might imply that the penetration depth estimation in this study is close to the real penetration depth. Thus, we believe that the impact of the X-band penetration depth is not enough to subvert the current results.

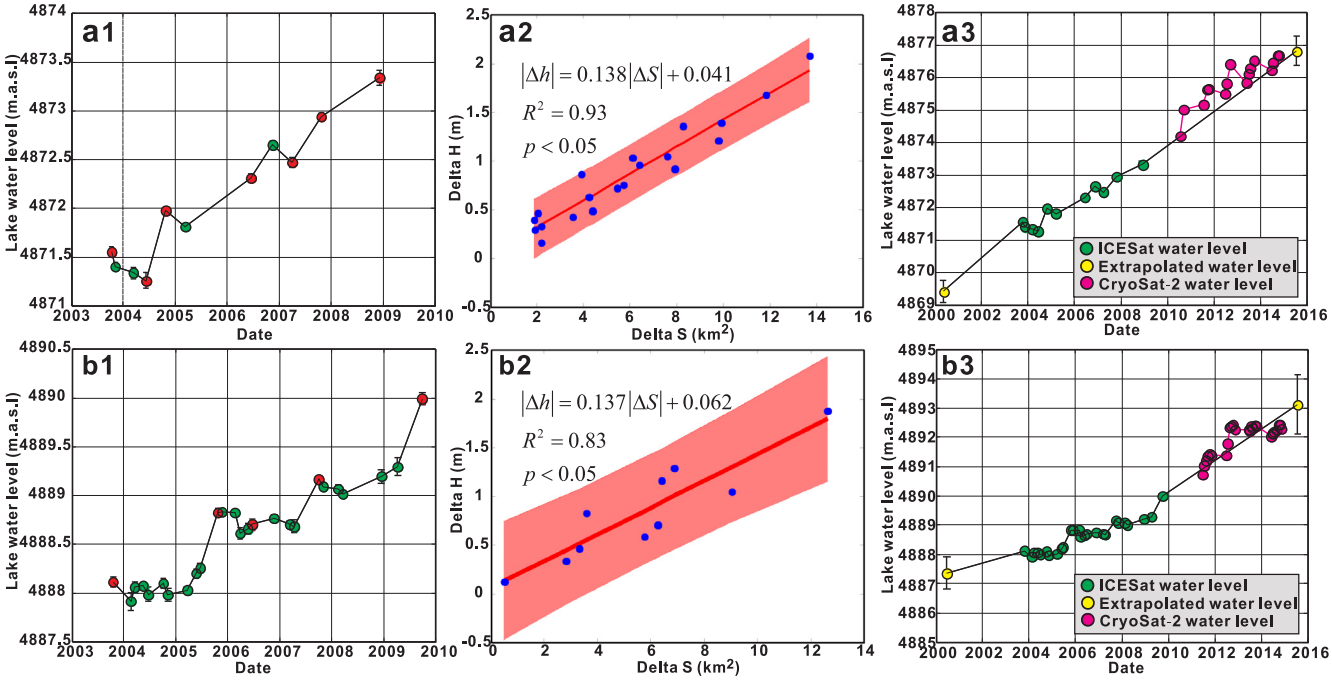

Fig. 5. Lake water-level changes for 2003–2008/09 (left); linear regression models linking the area change and the water-level change (middle); lake water-level changes for 2000–2015 (right). The labels of "a" and "b" represent LexieWudan Lake and Kekexili Lake, respectively. Note also that the data used to make a regression analysis are marked in red (in the left picture). The area shaded in pink (in the middle picture) represents the prediction interval of the linear regression model. (For interpretation of the references to color in this figure legend, the reader is referred to the web version of this article.)

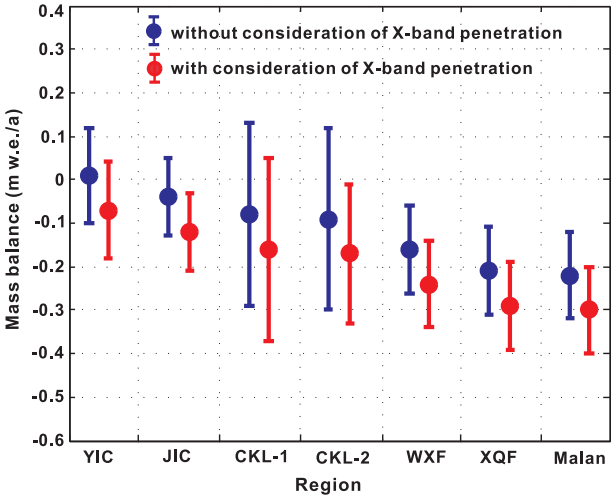

Fig. 6. Comparison of glacier mass balance between our results (blue) and additional results (red). Note that the abbreviations in the horizontal axis reflect the names of the study regions: YIC (YulangGangri Ice Cap), JIC (JinyangGangri Ice Cap), WXF (Wuxuefeng Mountain), XQF (Xinqingfeng Mountain). (For interpretation of the references to color in this figure legend, the reader is referred to the web version of this article.)

6.2. Comparison with previous mass balance studies

With regard to the glacier mass balance, our result of −0.16 ± 0.05 m w.e./a in the whole study region (for 2000–2015) is comparable to the ICESat-based estimate of Phan et al. (2017) (0.03 ± 0.47 m/a for 2003–2009) when considering the error bars, but clearly disagrees with that of Neckel et al. (2014) (−0.77 ± 0.35 m w.e./a for 2003–2009), despite the fact that our study period is twice as long. Furthermore, for the same or similar study period, a detailed comparison of our results with those of Brun et al. (2017) (2000–2016) shows that the differences of the mass balance are between −0.03 and 0.03 m w.e./a for individual sampling regions, and only 0.01 m w.e./a for the whole regions (Table 4). This indicates that the two results are compatible, given the error bounds. In addition, due to that Brun et al.'s (2017) results are not affected by the radar penetration depths, the comparison also confirms our speculation with respect to the limited impact of the X-band penetration depth in this study. In addition, through a comparison of the pattern of the glacier elevation change between Brun et al. (2017) and this study, we can speculate that this study region likely lies in a transition zone from negative to near-zero or positive mass balance for the whole of the Kunlun Mountains. This is because the glaciers from the YulangGangri Ice Cap toward the west along the Kunlun mountains have shown a positive mass balance (see Fig. 2a in Brun et al. (2017)). This can also be confirmed by the findings of Neckel et al. (2014) and Phan et al. (2017).

Table 4
Comparison of the glacier mass balance between this study and Brun et al. (2017) (unit: m w.e/a).

Region	This study	Brun et al. (2017)
CKL-1	−0.08 ± 0.21	−0.05 ± 0.07
CKL-2	−0.09 ± 0.16	−0.12 ± 0.07
YulangGangri	0.01 ± 0.11	−0.02 ± 0.07
Xinqingfeng	−0.21 ± 0.10	−0.19 ± 0.07
Malan	−0.22 ± 0.10	−0.20 ± 0.07
Wuxuefeng	−0.16 ± 0.10	N/A
JinyangGngri	−0.04 ± 0.09	−0.02 ± 0.07
All regions (area-weighted)	−0.16 ± 0.05	−0.15 ± 0.04

6.3. Comparison of different regression models for lake water-level extrapolation

To further validate the effectiveness and reliability of our models used to extrapolate water level, we re-estimated the water level in 2000 and 2015 by utilizing the first-order and second-order polynomial fit of the lake area versus the lake water level, respectively. Meanwhile, with

Table 5
Comparison of the extrapolated lake water levels based on different regression models.

Region	Model	No. measurements	R^2	Estimated water level (m)		Reference water level (m)	Difference(m)
				2000	2015		
LexieWudan	$L = 0.145S + 4837.357$	7	0.984	4869.31 ± 0.52	4876.80 ± 0.73	4876.67 ± 0.02(20/10/2014)	+0.13
	$L = 0.003S^2 - 1.476S + 5032.555$	7	0.992	4870.58 ± 1.87	4880.13 ± 4.81		+3.46
	$\|\Delta L\| = 0.138 \|\Delta S\| + 0.041$	21	0.929	4869.42 ± 0.34	4876.82 ± 0.45		+0.15
KekeXili	$L = 0.145S + 4842.558$	5	0.956	4887.25 ± 0.89	4893.66 ± 1.94	4892.44 ± 0.02(18/10/2014)	+1.22
	$L = 0.007S^2 - 4.114S + 5522.065$	5	0.996	4887.98 ± 0.86	4900.79 ± 7.22		+8.35
	$\|\Delta L\| = 0.137 \|\Delta S\| + 0.062$	10	0.831	4887.36 ± 0.55	4893.12 ± 1.00		+0.68

the CryoSat-2 observation in 2014 as the reference, we made a comparison for all results. In Table 5, we can see that if only from the angle of the model selection, the second-order polynomial model for the two lakes seems to be preferable, as its coefficient of determination (R^2) is larger than others. Nevertheless, the final results show that, for 2015, the estimated water levels based on the second-order model are 3.46 m (LexieWudan Lake) and 8.35 m (KekeXili Lake) higher than the reference value, respectively. Clearly, such significant water level change within one year is impossible and the estimates are totally erroneous. This can be confirmed by comparing optical images, which shows only a weak expansion in these two lakes for 2014–2015. In contrast, the results calculated by the two linear models, overall, are comparable to the reference water level. For example, in LexieWudan Lake, the differences between the extrapolated water level and the reference data are 0.13 m and 0.15 m, respectively, which are lower than the average rate of 0.50 m/a (for 2003–2014). This may be caused by the systematic bias between the ICESat and CryoSat-2 datasets (Fig. 5). Meanwhile, the difference of 0.02 m between the estimated results suggests that the performance of the two linear model is similar in this lake. However, it should be highlighted that the extrapolation accuracy of our linear model is higher, with a relatively low uncertainty (e.g., 0.45 m versus 0.73 m (Table 5)). This is because in the same conditions, the increase in the number of independent observations can enhance the robustness and reliability of the model prediction. Similarly, for KekeXili Lake, the differences of the estimated results versus reference water level are 1.22 m and 0.68 m, respectively. Given the latter is very close to the rate of water-level rise of 0.50 m/a (for 2007–2014), our result is more reasonable and reliable. Meanwhile, this also indicates that our model is optimal (at least in this lake), as another linear model (using the lake area and the water level as parameters) generates an overestimated result. In addition, with regard to the lake water level estimation in 2000, considering the performance of our models discussed above, we believe that our results are more accurate, in spite of the lack of reference data. In conclusion, the models of lake water-level extrapolation we used are effective and the results can be considered as reliable and acceptable.

6.4. Analysis of the contribution of glacier meltwater and the potential driving forces of lake changes

In this study, with regard to the contribution of glacier meltwater to lake expansion, since we did not consider the mass loss caused by the evaporation and sublimation process in the glacier systems and the transfer wastage (i.e., evaporation, percolation loss) in the process of runoff flow, our results represent a maximum contribution (or an upper bound). This means that, in the LexieWudan Lake and KekeXili Lake basins, the contributions from glacier mass loss were no more than 9.9% and 11.1% between 2000 and 2015, respectively, revealing a limited impact on lake water storage change. If we assume a glacier runoff coefficient of 0.6 (Wu et al., 2014a), then the contributions are only 5.9% and 6.66%. The estimates are comparable to the findings for the central Tibetan Plateau (Lei et al., 2013; Li et al., 2017a; Tong et al., 2016), despite the conditions of each lake basin being different (e.g., the ratio of glacier area to lake area, and the ratio of basin area to lake area). For example, based on the same method as this study, Lei et al. (2013) reported that the glacier mass loss for 1999–2010 accounted for about 11.7%, 28.7%, and 11.4% of the lake water-level rise for Seling Co Lake, Nam Co Lake, and Pung Co Lake, respectively. Updated results obtained by physical-based models revealed that the glacier mass loss accounted for only about 10% of the water-level rise in Nam Co Lake (for 1961–2015) (Li et al., 2017a) and 5% in Seling Co Lake (for 1979–2013) (Tong et al., 2016). In addition, for the whole endorheic basin of the QTP, Zhang et al. (2017) revealed that the contribution of glacier mass loss to lake volume increase is only 13% from the 1970s to 2015, which is basically consistent with our estimates.

For the variation of the lakes, in this study region, meteorological data suggested that both the annual precipitation and annual mean air temperature exhibited an increasing trend for 1960–2010, e.g., at a rate of 0.79 °C/(10 a) and 18.84 mm/(10 a), respectively (Jiang et al., 2012), while the potential evaporation showed a decrease of −1.10 mm/a for 1970–2011 (Yao et al., 2013). The increased precipitation and decreased evaporation were considered to be the main causes of the lake water-level rise (Yao et al., 2013). Nevertheless, some recent studies have shown that the dominant driving forcing behind the lake growth is merely the increased precipitation (Tong et al., 2016; Yang et al., 2017; Lei et al., 2017; Zhang et al., 2017). For instance, in Seling Co Lake, the precipitation-induced runoff accounts for 82% of the increase in the mean annual water input (Tong et al., 2016). On the whole plateau scale, the increased net precipitation increase accounts for 74% of lake storage increase, while the contribution of the permafrost thaw recharge is only 12% (Zhang et al., 2017). Based on these, we can speculate that the increased precipitation may be the decisive driving force of lake growth in this study region.

7. Conclusion

In this study, based on the geodetic method, we calculated the region-wide glacier mass balance for 2000–2015/16 in the central Kunlun-KekeXili region (including seven sample regions) using SPOT-6/7 stereo imagery and the SRTM DEM. The results reflect a heterogeneous pattern at the sub-region spatial scale. The most significant glacier mass loss, at rates of −0.22 ± 0.10 and −0.21 ± 0.10 m w.e./a, occurred in the Malan and Xinqingfeng mountains, respectively. Moreover, except for the YulangGangri Ice Cap with a near-zero mass balance of 0.01 ± 0.11 m w.e./a., the other regions (i.e., JinyangGangri Ice Cap and the Wuxuefeng and central Kunlun mountains) experienced slight or moderate mass loss, with a mass balance range of −0.04 ± 0.09 m w.e./a to −0.16 ± 0.10 m w.e./a. The area-weighted glacier mass balance is −0.16 ± 0.05 m w.e./a for the whole region. In addition, we evaluated the water storage change of two glacier-fed closed lakes for 2000–2015, based on the function relationship between water level change and area change. The results showed that the water storage of LexieWudan Lake and KekeXili Lake increased by 1.82 ± 0.14 km^3 and 1.90 ± 0.38 km^3, respectively. Meanwhile, within the two lake basins, the water lost from the glaciers was −0.18 ± 0.03 km^3 and −0.21 ± 0.04 km^3, indicating that the

contributions of glacier mass loss to lake expansion were no more than 9.9% and 11.1% in LexieWudan Lake and KekeXili Lake, respectively. From a quantitative point of view, this demonstrates that glacier meltwater is not the dominant influencing factor for the lake expansion in the northern part of the QTP.

Declaration of Interest statement

None.

Acknowledgments

We are grateful to Dr. Jiang Liguang of the Technical University of Denmark for providing the CryoSat-2 results and giving some constructive suggestions as to how we could improve this manuscript. The Second Chinese Glacier Inventory was provided by the Environmental and Ecological Science Data Center for West China (http://westdc.westgis.ac.cn). The SRTM C-band DEM and the Landsat 5/7/8 images were freely downloaded from the USGS. We would also like to thank the DLR for providing the SRTM X-band DEM and the NDSIC for freely providing the ICESat GLA14 data. This research was funded by the National Natural Science Foundation of China (grant numbers: 41474007, 41574005), the Project of Innovation-driven Plan of Central South University (grant number: 2016CX004), and the Fundamental Research Funds for the Central Universities of Central South University (grant number: 2017zzts173).

Appendix A. Supplementary data

Supplementary data to this article can be found online at https://doi.org/10.1016/j.jhydrol.2019.01.007.

References

Abdallah, H., Bailly, J.S., Baghdadi, N., Lemarquand, N., 2011. Improving the assessment of ICESat water altimetry accuracy accounting for autocorrelation. ISPRS J. Photogramm. Remote Sens. 66 (6), 833–844.

Berthier, E., Arnaud, Y., Kumar, R., Ahmad, S., Wagnon, P., Chevallier, P., 2007. Remote sensing estimates of glacier mass balances in the Himachal Pradesh (Western Himalaya, India). Remote Sens. Environ. 108 (3), 327–338.

Berthier, E., Cabot, V., Vincent, C., Six, D., 2016. Decadal region-wide and glacier-wide mass balances derived from multi-temporal ASTER satellite digital elevation models. Validation over the Mont-Blanc area. Front. Earth Sci. 4. https://doi.org/10.3389/feart.2016.00063.

Brun, F., Berthier, E., Wagnon, P., Kääb, A., Treichler, D., 2017. A spatially resolved estimate of High Mountain Asia glacier mass balances from 2000 to 2016. Nat. Geosci. 10 (9), 668–673. https://doi.org/10.1038/NGEO2999.

Crétaux, J.F., Abarca-del-Río, R., Berge-Nguyen, M., Arsen, A., Drolon, V., Clos, G., Maisongrande, P., 2016. Lake volume monitoring from space. Surv. Geophys. 37 (2), 269–305.

Dehecq, A., Millan, R., Berthier, E., Gourmelen, N., Trouve, E., 2016. Elevation changes inferred from TanDEM-X data over the Mont-Blanc area: Impact of the X-band interferometric bias. IEEE J. Sel. Top. Appl. Earth Obs. Remote Sens. 9, 3870–3882. https://doi.org/10.1109/JSTARS.2016.2581482.

Duan, Z., Bastiaanssen, W.G.M., 2013. Estimating water volume variations in lakes and reservoirs from four operational satellite altimetry databases and satellite imagery data. Remote Sens. Environ. 134, 403–416.

Farr, T.G., Rosen, P.A., Caro, E., Crippen, R., Duren, R., Hensley, S., et al., 2007. The shuttle radar topography mission. Rev. Geophys. 45 (2). https://doi.org/10.1029/2005RG000183.

Gardelle, J., Berthier, E., Arnaud, Y., Kääb, A., 2013. Region-wide glacier mass balances over the Pamir-Karakoram-Himalaya during 1999–2011. The Cryosphere 7, 1263–1286. https://doi.org/10.5194/tc-7-1263-2013.

Gardner, A.S., Moholdt, G., Cogley, J.G., Wouters, B., Arendt, A.A., Wahr, J., Berthier, E., Hock, R., Pfeffer, W.T., Kaser, G., Ligtenberg, S.R.M., Bolch, T., Sharp, M.J., Hagen, J.O., van den Broeke, M.R., Paul, F., 2013. A reconciled estimate of glacier contributions to sea level rise: 2003 to 2009. Science 340, 852–857. https://doi.org/10.1126/science.1234532.

Groh, A., Ewert, H., Rosenau, R., Fagiolini, E., Gruber, C., Floricioiu, D., Abdel Jaber, W., Linow, S., Flechtner, F., Eineder, M., Dierking, W., Dietrich, R., 2014. Mass, volume and velocity of the antarctic ice sheet: present-day changes and error effects. Surv. Geophys. 35, 1481–1505. https://doi.org/10.1007/s10712-014-9286-y.

Guo, W., Liu, S., Xu, J., Wu, L., Shangguan, D., Yao, X., Wei, J., Bao, W., Yu, P., Liu, Q., Jiang, Z., 2015. The second Chinese glacier inventory: data, methods and results. J. Glaciol. 61, 357–372. https://doi.org/10.3189/2015JoG14J209.

Huss, M., 2013. Density assumptions for converting geodetic glacier volume change to mass change. Cryosphere 7, 877–887. https://doi.org/10.5194/tc-7-877-2013.

Höhle, J., Höhle, M., 2009. Accuracy assessment of digital elevation models by means of robust statistical methods. ISPRS J. of Photogramm. Rem. Sens. 64, 398–406. https://doi.org/10.1016/j.isprsjprs.2009.02.003.

Jiang, L., Nielsen, K., Andersen, O.B., Bauer-Gottwein, P., 2017. Monitoring recent lake level variations on the Tibetan Plateau using CryoSat-2 SARIn mode data. J. Hydrol. 544, 109–124.

Jiang, S., Yang, T., Tian, H., 2012. Glacier shrinkage and its dependence on climate in the Malan mountain in past 40 years based on RS and GIS. J. Glaciol. Geocryol. 34 (3), 522–529 (In Chinese, with the abstract in English).

Kääb, A., Treichler, D., Nuth, C., Berthier, E., 2015. Brief Communication: Contending estimates of 2003–2008 glacier mass balance over the Pamir–Karakoram–Himalaya. Cryosphere 9, 557–564. https://doi.org/10.5194/tc-9-557-2015.

Kääb, A., Leinss, S., Gilbert, A., Bühler, Y., Gascoin, S., Evans, S.G., Bartelt, P., Berthier, E., Brun, F., Chao, W., Farinotti, D., Gimbert, F., Guo, W., Huggel, C., Kargel, J., Leonard, G., Tian, L., Treichler, D., Yao, T., 2018. Massive collapse of two glaciers in western Tibet in 2016 after surge-like instability. Nat. Geosci. 11 (2), 114.

Lei, Y., Yao, T., Yi, C., Wang, W., Sheng, Y., Li, J., Joswiak, D., 2012. Glacier mass loss induced the rapid growth of Linggo Co on the central Tibetan Plateau. J. Glaciol. 58 (207), 177–184.

Lei, Y., Yao, T., Bird, B.W., Yang, K., Zhai, J., Sheng, Y., 2013. Coherent lake growth on the central Tibetan Plateau since the 1970s: Characterization and attribution. J. Hydrol. 483, 61–67.

Lei, Y., Yang, K., Wang, B., Sheng, Y., Bird, B.W., Zhang, G., Tian, L., 2014. Response of inland lake dynamics over the Tibetan Plateau to climate change. Clim. Change 125 (2), 281–290.

Lei, Y., Yao, T., Yang, K., Sheng, Y., Kleinherenbrink, M., Yi, S., Brid, B.W., Zhang, X., Zhu, L., Zhang, G., 2017. Lake seasonality across the Tibetan Plateau and their varying relationship with regional mass changes and local hydrology. Geophys. Res. Lett. 44 (2), 892–900.

Leprince, S., Ayoub, F., Klingert, Y., Avouac, J.-P., 2007. Co-Registration of Optically Sensed Images and Correlation (COSICorr): an operational methodology for ground deformation measurements. In: Geoscience and Remote Sensing Symposium, 2007, IGARSS 2007. IEEE International, 1943–1946. https://doi.org/10.1109/IGARSS.2007.4423207.

Li, B.Y., Gu, G.A., Li, S.D., 1996. Physical environment of HohXil region, Qinghai. The comprehensive scientific expedition to the Hoh Xil region (in Chinese). Science Press, Beijing, China.

Li, B., Zhang, J., Yu, Z., Liang, Z., Chen, L., Acharya, K., 2017a. Climate change driven water budget dynamics of a Tibetan inland lake. Global Planet. Change 150, 70–80.

Li, J., Li, Z.W., Zhu, J.J., Li, X., Xu, B., Wang, Q.J., Huang, C.L., Hu, J., 2017b. Early 21st century glacier thickness changes in the Central Tien Shan. Remote Sens. Environ. 192, 12–29. https://doi.org/10.1016/j.rse.2017.02.003.

Liu, S.Y., Guo, W.Q., Xu, J.L., Shangguan, D.H., Wu, L.Z., Yao, X.J., Zhao, J.D., Liu, Q., Jiang, Z.L., Li, P., Wei, J.F., Bao, W.J., Yu, P.C., Ding, L.F., Li, G., Ge, C.M., Wang, Y.. The Second Glacier Inventory Dataset of China (Version 1.0). Cold and Arid Regions Science Data Center at Lanzhou, 2014. http://dx.doi:10.3972/glacier.001.2013.db.

Lambrecht, A., Mayer, C., Wendt, A., Floricioiu, D., Völksen, C., 2018. Elevation change of Fedchenko Glacier, Pamir Mountains, from GNSS field measurements and TanDEM-X elevation models, with a focus on the upper glacier. J. Glaciol. 1–12.

Ludwig, R., Schneider, P., 2006. Validation of digital elevation models from SRTM X-SAR for applications in hydrologic modeling. ISPRS J. Photogramm. Remote Sens. 60 (5), 339–358.

Maurer, J.M., Rupper, S.B., Schaefer, J.M., 2016. Quantifying ice loss in the eastern Himalayas since 1974 using declassified spy satellite imagery. Cryosphere 10, 2203. https://doi.org/10.5194/tc-10-2203-2016.

Neckel, N., Kropáček, J., Bolch, T., Hochschild, V., 2014. Glacier mass changes on the Tibetan Plateau 2003–2009 derived from ICESat laser altimetry measurements. Environ. Res. Lett. 9 (1), 014009.

Nuth, C., Kääb, A., 2011. Co-registration and bias corrections of satellite elevation data sets for quantifying glacier thickness change. Cryosphere 5, 271–290. https://doi.org/10.5194/tc-5-271-2011.

Phan, V.H., Lindenbergh, R., Menenti, M., 2012. ICESat derived elevation changes of Tibetan lakes between 2003 and 2009. Int. J. Appl. Earth Obs. Geoinf. 17, 12–22.

Phan, V.H., Lindenbergh, R., Menenti, M., 2017. Assessing orographic variability in glacial thickness changes at the Tibetan Plateau using Icesat laser altimetry. Remote Sensing 9 (2), 160.

Ragettli, S., Bolch, T., Pellicciotti, F., 2016. Heterogeneous glacier thinning patterns over the last 40 years in Langtang Himal. The Cryosphere 10, 2075–2097.

RGI Consortium Randolph Glacier Inventory – A Dataset of Global Glacier Outlines: Version 6.0: Technical Report, Global Land Ice Measurements from Space 2017 Digital Media Colorado, USA 10.7265/N5-RGI-60.

Rignot, E., Echelmeyer, K., Krabill, W., 2001. Penetration depth of interferometric synthetic-aperture radar signals in snow and ice. Geophys. Res. Lett. 28, 3501–3504. https://doi.org/10.1029/2000GL012484.

Rolstad, C., Haug, T., Denby, B., 2009. Spatially integrated geodetic glacier mass balance and its uncertainty based on geostatistical analysis: application to the western Svartisen ice cap. Norway. J. Glaciol. 55, 666–680. https://doi.org/10.3189/002214309789470950.

Roth, A., Eineder, M., Rabus, B., Mikusch, E., Schättler, B., 2001. SRTM/X-SAR: products and processing facility. In: Geoscience and Remote Sensing Symposium, 2001. IGARSS'01, vol. 2. IEEE 2001 International, pp. 745–747.

Round, V., Leinss, S., Huss, M., Haemmig, C., Hajnsek, I., 2017. Surge dynamics and lake outbursts of Kyagar Glacier, Karakoram. The Cryosphere 11 (2), 723–739.

Seehaus, T., Marinsek, S., Helm, V., Skvarca, P., Braun, M., 2015. Changes in ice

dynamics, elevation and mass discharge of Dinsmoor-Bombardier-Edgeworth glacier system, Antarctic Peninsula. Earth Planet. Sci. Lett. 427, 125–135. https://doi.org/10.1016/j.epsl.2015.06.047.
Song, C., Huang, B., Ke, L., 2013. Modeling and analysis of lake water storage changes on the Tibetan Plateau using multi-mission satellite data. Remote Sens. Environ. 135, 25–35.
Song, C., Huang, B., Ke, L., 2014a. Inter-annual changes of alpine inland lake water storage on the Tibetan Plateau: detection and analysis by integrating satellite altimetry and optical imagery. Hydrol. Process. 28 (4), 2411–2418.
Song, C., Huang, B., Richards, K., Ke, L., Hien Phan, V., 2014b. Accelerated lake expansion on the Tibetan Plateau in the 2000s: induced by glacial melting or other processes? Water Resour. Res. 50 (4), 3170–3186.
Song, C., Ye, Q., Sheng, Y., Gong, T., 2015a. Combined ICESat and CryoSat-2 altimetry for accessing water level dynamics of Tibetan lakes over 2003–2014. Water 7 (9), 4685–4700.
Song, C., Ye, Q., Cheng, X., 2015b. Shifts in water-level variation of Namco in the central Tibetan Plateau from ICESat and CryoSat-2 altimetry and station observations. Science bulletin 60 (14), 1287–1297.
SPOT-6/7 imagery User Guide. Available on: www.intelligence-airbusds.com/en/8577-spot-6-user-guide-download.
Tong, K., Su, F., Xu, B., 2016. Quantifying the contribution of glacier meltwater in the expansion of the largest lake in Tibet. J. Geophys. Res.: Atmos. 121 (19).
Wang, X., Gong, P., Zhao, Y., Xu, Y., Cheng, X., Niu, Z., Luo, Z., Huang, H., Sun, F., Li, X., 2013. Water-level changes in China's large lakes determined from ICESat/GLAS data. Remote Sens. Environ. 132, 131–144.
Wu, H., Wang, N., Jiang, X., Guo, Z., 2014a. Variations in water level and glacier mass balance in Nam Co lake, Nyainqentanglha range, Tibetan Plateau, based on ICESat data for 2003–09. Ann. Glaciol. 55, 239–247. https://doi.org/10.3189/2014AoG66A100.
Wu, Y., Zheng, H., Zhang, B., Chen, D., Lei, L., 2014b. Long-term changes of lake level and water budget in the Nam Co Lake Basin, central Tibetan Plateau. J. Hydrometeorol. 15 (3), 1312–1322.
Xie, Z.C., Han, J.K., Feng, Q.H., Wang, X.J., 2000. Primary study on the glaciers of Mountain Malan, HohXil region, Qinghai-Xizang Plateau. J. Nat. Sci. Hunan Normal Univ. 23 (1), 83–88 (In Chinese).
Xie, Z.C., Liu, C.H., 2010. Introduction of Glaciology (in Chinese). Science Press, Beijing, China.
Yao, T., Thompson, L., Yang, W., Yu, W., Gao, Y., Guo, X., Yang, X., Duan, K., Zhao, H., Xu, B., Pu, J., Lu, A., Xiang, Y., Kattel, D.B., Joswiak, D., 2012. Different glacier status with atmospheric circulations in Tibetan Plateau and surroundings. Nat. Clim. Change 2, 663–667. https://doi.org/10.1038/nclimate1580.
Yao, X., Liu, S., Li, L., Sun, M., Luo, J., Feng, Y., 2013. Spatial-temporal variations of lake area in HohXil region in the past 40 years. Acta Geog. Sinica 68 (7), 886–896 (In Chinese, with the abstract in English).
Yang, K., Yao, F., Wang, J., Luo, J., Shen, Z., Wang, C., Song, C., 2017. Recent dynamics of alpine lakes on the endorheic Changtang Plateau from multi-mission satellite data. J. Hydrol. 552, 633–645.
Zhang, G., Xie, H., Kang, S., Yi, D., Ackley, S.F., 2011. Monitoring lake level changes on the Tibetan Plateau using ICESat altimetry data (2003–2009). Remote Sens. Environ. 115 (7), 1733–1742.
Zhang, G., Xie, H., Yao, T., Kang, S., 2013a. Water balance estimates of ten greatest lakes in China using ICESat and Landsat data. Chin. Sci. Bull. 58 (31), 3815–3829.
Zhang, G., Yao, T., Xie, H., Kang, S., Lei, Y., 2013b. Increased mass over the Tibetan Plateau: from lakes or glaciers? Geophys. Res. Lett. 40 (10), 2125–2130.
Zhang, G., Yao, T., Shum, C.K., Yi, S., Yang, K., Xie, H., Feng, W., Bolch, T., Wang, L., Behrangi, A., Zhang, H., Wang, W., Xiang, Y., Yu, J., 2017. Lake volume and groundwater storage variations in Tibetan Plateau's endorheic basin. Geophys. Res. Lett. 44 (11), 5550–5560.
Zhao, J., Floricioiu, D., 2017. The penetration effects on TanDEM-X elevation using the GNSS and laser altimetry measurements in Antarctica. Int. Arch. Photogramm., Remote Sens. Spatial Inf. Sci. 42, 1593.
Zhou, Y., Li, Z., Li, J., 2017. Slight glacier mass loss in the Karakoram region during the 1970s to 2000 revealed by KH-9 images and SRTM DEM. J. Glaciol. 63 (238), 331–342.
Zhou, Y., Li, Z., Li, J., Zhao, R., Ding, X., 2018. Glacier mass balance in the Qinghai-Tibet Plateau and its surroundings from the mid-1970s to 2000 based on Hexagon KH-9 and SRTM DEMs. Remote Sens. Environ. 210, 96–112.
Zwally, H.J., Schutz, B., Abdalati, W., Abshire, J., Bentley, C., Brenner, A., Bufton, J., Dezio, J., Hancock, D., Harding, D., Herring, T., Minster, B., Quinn, K., Palm, S., Spinhirne, J., Thomas, R., 2002. ICESat's laser measurements of polar ice, atmosphere, ocean, and land. J. Geodyn. 34 (3–4), 405–445.
Zwally, H.J., Yi, D., Kwok, R., Zhao, Y., 2008. ICESat measurements of sea ice freeboard and estimates of sea ice thickness in the Weddell Sea. J. Geophys. Res. Oceans 113 (C2).